ACS APPLIED MATERIALS & INTERFACES

www.acsami.org

Research Article

Scalable, Alternating Narrow Stripes of Polyvinyl Alcohol Support and Unmodified PEDOT:PSS with Maintained Conductivity Using a Single-Step Slot Die Coating Approach

Ara W. Parsekian and Tequila A. L. Harris*

Cite This: *ACS Appl. Mater. Interfaces* 2020, 12, 3736–3745

Read Online

ACCESS | Metrics & More | Article Recommendations

ABSTRACT: Slot die coating has been established as an economical approach for deposition of parallel narrow stripes, a constituent pattern feature in many printed device applications. However, the minimum feature size that can be achieved using this approach is constrained by wetting and liquid bridge phenomena at the deposition region. We hypothesize that pattern resolution and process control can be improved by co-depositing a support fluid to stabilize the pattern. Electrically conductive poly(3,4-ethylenedioxythiophene):polystyrene sulfonate (PEDOT:PSS) is slot die-coated in parallel stripes on flexible poly(ethylene terephthalate) substrate, without wettability-enhancing dopants or substrate pretreatment. A miscible liquid phase, polyvinyl alcohol, is used as the support material. Feature size performance and conductivity of PEDOT:PSS stripe regions are evaluated across a range of process conditions. Narrow PEDOT:PSS stripes produced using our technique range from 400 to 850 μm and exhibit conductivity approaching 1.5 S cm^{-1}. This electrical performance falls within the upper range expected prior to standard conductivity-enhancing post-treatments. Significantly, dewetting effects normally present with undoped PEDOT:PSS on the plastic substrate are fully mitigated with our deposition technique. These results indicate high ease of processing and good feature size performance, with few inherent drawbacks to the functional properties of the patterned films.

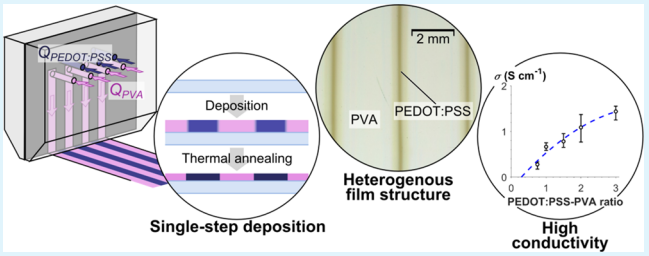

KEYWORDS: *printed electronics, flexible, roll-to-roll, slot die coating, PEDOT:PSS, feature size*

1. INTRODUCTION

For emerging flexible thin film devices, solution coating techniques have long been appreciated as a route to fast and economical roll-to-roll (R2R) manufacturing.[1,2] While the broad variety of materials and structures used in thin film devices continues to expand, the fluid rheology and wetting requirements for modern solution coating techniques remain influential in material formulation.[3−7] Furthermore, physical deposition of patterned films is frequently reliant on substrate prepatterning,[8−12] pattern masks,[13−16] or postdeposition subtractive steps[17−19] as reported in recent literature. Although these approaches are often feasible, they present challenges for large-scale manufacturing where process simplicity and device cost are leading considerations. This has motivated interest in developing methods for direct single-step pattern deposition, without significant process-imposed requirements on material formulation, to facilitate the broad practical impact of patterned thin film devices.[2,20−22]

Single-step deposition of complex features has previously been demonstrated using a variety of printing techniques such as flexography,[23−25] gravure printing,[26,27] screen printing,[28−30] inkjet,[31−43] and aerosol,[44,45] as well as meniscus guide coating methods including direct-write,[46−48] blade coating,[49−51] solution shearing,[52−55] and slot die coating.[4,56−66] Meniscus guide techniques offer unique possibilities for control over pattern morphology, film crystallinity, and microstructure alignment through viscous shear, evaporation, and controlled wetting phenomena.[20,22,67] On the other hand, printing-derived approaches are widely recognized as most suitable for high-throughput deposition across a wide area.[4,5,68,69]

Slot die coating has received particular interest as a meniscus guide technique that also exhibits suitability for wide area, large-scale manufacturing. Thus, despite its limited patterning capability compared to competing printing methods, slot coating has been used on numerous occasions to demonstrate manufacturing feasibility for printed devices such as solar cell modules,[19,21,56,58−61,70] batteries,[60,71] and organic light-emitting diodes.[72,73] While these devices can easily be fabricated as narrow stripes of width and spacing greater than 1 mm, smaller feature sizes have proven to be a persistent challenge for

Received: October 19, 2019
Accepted: December 27, 2019
Published: December 27, 2019

https://dx.doi.org/10.1021/acsami.9b18936
ACS Appl. Mater. Interfaces 2020, 12, 3736–3745

conventional slot die coating.[4,56−62] This limitation on patterning resolution is consequential because it precludes a wide range of micro-stripe devices that would otherwise be well-suited to the technique. These include optical waveguides,[74] diffraction gratings,[75] color filters[39] field-effect transistors,[43,54,76,77] microfluidic devices,[42] strain gauge sensors,[40] and two-dimensional interdigitated capacitors.[78]

Recent efforts to improve the patterning resolution of slot die coating have achieved stripes as narrow as 377 μm using a flow-actuated slot die coater,[79] and 168 μm using a shim mask and meniscus guide with 150 μm-wide micro-tips.[73] Slot coating has also been adapted for deposition of curved regions[63] and regular patches,[64−66] as well as digital patterning of arbitrary shapes,[79] although this approach is still in its early infancy compared to inkjet, aerosol, and similar established printing methods. Despite these advances, slot coating-inspired approaches continue to face several practical obstacles. First, the potential for unwanted coalescence of adjacent stripes deposited in a single tool pass creates a significant trade-off between feature size and process yield.[73,79] Furthermore, because pattern generation is mediated by meniscus behavior and post-deposition spreading, process capability is strongly tied to the physical properties of the coating material, substrate, and slot die tool.[59,64,79,80] Resolution performance of the process is limited by the smallest achievable meniscus between the coating tool and substrate,[80] and strategies to control post-deposition spreading require significant process characterization in the absence of substrate wettability enhancements.[37,38,80]

In this work, a single-step slot die coating technique for heterogeneous narrow-stripe patterns is introduced and demonstrated with feature sizes below 1 mm. The technique is unique[81] in its ability to process materials that suffer from dewetting defects with conventional solution processing methods, by virtue of a support fluid codeposited with the stripe pattern. The technique offers a significantly consolidated process flow relative to established deposition techniques commonly used to fabricate stripe-patterned composite films comprising two materials.[5,22,77,81,82] Here, poly(3,4-ethylenedioxythiophene):polystyrene sulfonate (PEDOT:PSS), a widely used transparent hole injection[30,58,83−85] and electrochromic layer material,[50,86−88] is deposited in aqueous dispersion on flexible poly(ethylene terephthalate) (PET) substrate, without additional wettability-enhancing dopants as required in previous studies with similar materials.[4,25,58,73,79,89−92] Polyvinyl alcohol (PVA), a nonhazardous dielectric barrier and mask material in other printed composite films,[43,93] is codeposited in aqueous solution as a support material defining the conductive stripe pattern. The resulting process control over pattern morphology and film thickness is investigated and compared to the conventional approach using slot die coating. Briefly, the role of wetting and mixing in the deposition of stable and functional patterns is considered. Finally, the electrical performance of thermally annealed films is characterized in terms of deposition conditions and pattern structures.

2. MATERIALS AND METHODS

2.1. Materials. PEDOT:PSS (1.0−1.3 wt % aqueous), Clevios PH-1000 purchased from Heraeus GmbH, was filtered prior to deposition, but otherwise used as received. PVA, Mowiol 4-88 from Sigma-Aldrich, was prepared in aqueous solution by continuous stirring for 30 min at 60 °C. PVA solutions were prepared at 10 wt % concentration, in order to match the viscosity of PEDOT:PSS dispersion. Heterogeneous films comprising PEDOT:PSS and PVA were deposited on flexible PET film (ES301400 purchased from Goodfellow Cambridge Ltd.). To evaluate miscibility, PVA solutions were prepared at 24 wt % concentration; polydimethylsiloxane (PDMS), Dow Corning 200 fluid purchased from Sigma-Aldrich Co., was used as-received; glycerol was purchased from EMD Chemicals Inc. at 99.5 wt % purity and prepared in a 95 wt % aqueous solution at 25 °C; and vacuum pump oil (VPO), L340 purchased from Virginia KMP Corporation, was used as received. The slot die coating tool was constructed from polymethyl methacrylate.

2.2. Wetting and Fluid Characterization. Advancing and receding contact angles (θ_a, θ_r), surface tension (γ), and liquid−liquid interfacial tension were measured on a model 500-U1 Ramé-Hart goniometer. For surface tension measurements of single fluids, the pendant drop method was used with disposable polytetrafluoroethylene (PTFE) syringe tips as the solid phase. For interfacial tension measurements, the outer liquid phase was contained in a Ramé-Hart quartz cell. Apparent contact angles were measured on PET film using the volume-add/volume-subtract method. Viscosity of aqueous PEDOT:PSS was measured with a Cannon-Fenske viscometer tube at 25 °C. Measured values for these material properties are organized in Table 1; where noted, some values were extracted from existing literature.

Table 1. Physical Properties of Coating Fluids at 25 °C

material	γ (mN m^{-1})	contact angle on PET (deg) θ_a	θ_r	μ (cP)
PEDOT:PSS	71	81	42	29
PVA (10 wt %)	44	67	0	26[b]
PVA (24 wt %)[a]	42			
glycerol[a]	63			
PDMS[a]	20			
VPO[a]	31			

[a]Appears only in wetting demonstrations in Section 3.2.3. [b]Reference 94.

2.3. Pattern Film Deposition. Alternating narrow stripes of PVA and PEDOT:PSS were deposited using the heterogeneous stripe slot coating approach, illustrated in Figure 1a, and narrow stripes of PVA were deposited using the conventional slot die approach illustrated in Figure 1c. All coating processes were carried out with a stationary slot coating tool positioned above the moving substrate, supported by a vacuum platen with a transparent borosilicate viewing window. A fixed slot gap (G) of 76 μm, slot die lip length (L) of 2.36 mm, outlet width (w_0) of 0.94 mm, and center-to-center outlet spacing (p_0) of 1.5 mm were used for all deposition trials. Both the total rate of flow through the slot die (Q) and flow rate-per-stripe ratio between fluid species ($Q_{PEDOT:PSS}/Q_{PVA}$) was controlled by two Chemyx Fusion 200 syringe pumps. To distribute metered flow among the multiple inlets, a separate manifold was used for each of the two fluids. Relative substrate velocity (V) and coating gap (H) between the tool and substrate were also varied across coating runs. The above process input parameters are illustrated schematically in Figure 1a. Immediately after deposition, films were subjected to drying and thermal annealing in an oven at 130 °C for 30 min, based on expected conductivity improvements for undoped PEDOT:PSS films, following similar annealing procedures in previous works.[24,58,83,95] Previous studies have shown that this conductivity improvement corresponds to solvent removal and reduction in film thickness rather than changes in the molecular structure of the PEDOT, below a temperature of around 300 °C.[96−98]

2.4. Coating Tool Description. The slot die coater used in this work is compared schematically with conventional slot die coating, alongside the corresponding process flow, in Figure 1. Coating fluid enters a die through an array of inlets and is deposited at localized

https://dx.doi.org/10.1021/acsami.9b18936
ACS Appl. Mater. Interfaces 2020, 12, 3736−3745

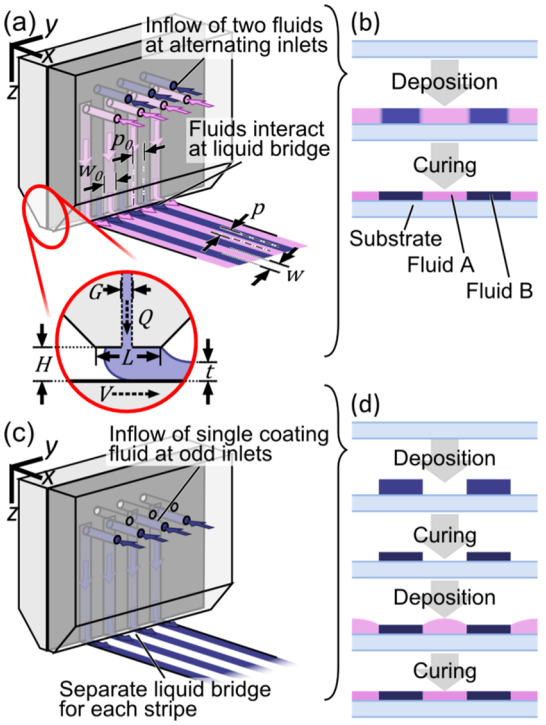

Figure 1. (a) Schematic of the heterogeneous stripe slot-coating approach and processing parameters, corresponding to the process flow in (b), compared to the conventional stripe slot coating approach with the same tooling (c) and resulting process flow with additional process steps (d).

deposition regions, with flow from each inlet kept separate within the tool. Injection of two coating fluid species in an alternating fashion, as illustrated in Figure 1a,b, produces the desired heterogeneous narrow-stripe pattern. The process flow for this approach comprises just two steps: deposition and thermal annealing. By contrast, the conventional slot die approach to narrow stripes, illustrated in Figure 1c,d, deposits only one type of coating fluid per tool pass and requires additional deposition and curing steps to achieve a heterogeneous narrow-stripe pattern. Where free-standing stripes are required, the heterogeneous stripe slot coating approach must be used in conjunction with subsequent process steps to remove the support material, if it cannot be retained because of decreased functionality or property changes. However, for many applications, a support material may be selected to provide useful functionality, such as a dielectric barrier between conductive regions,[43,48,52,53,93] as in this work. In other cases, it may be acceptable to leave the support material in place even if it provides no benefit beyond defining the narrow-stripe pattern.

The presence of the support material in the heterogeneous film also precludes unwanted coalescence of adjacent stripes. The coalescence defect has been highlighted previously for various meniscus guide coating methods, including the conventional slot die approach illustrated in Figure 1c,d, as a significant practical limitation on the minimum stripe spacing for wide-area coating.[73,79] By virtue of the support material codeposited between neighboring parallel stripes, the heterogeneous stripe slot coating approach illustrated in Figure 1a,b ensures that coalescence defects do not occur. While conventional approaches can be combined with selective wettability enhancements to the substrate to accomplish this same goal,[11,41,77,99] the approach in Figure 1a,b may be preferable where cost and simplicity of the manufacturing approach are critical.

It should be noted that this approach is distinct from the multilayer slot-coating approach outlined in previous literature,[4,65,100] which produces a vertically-stratified film rather than the alternating narrow-stripe structure across the stripe width, as shown in Figure 1a. To distinguish the technique presented here from "multimaterial" or "multilayer" slot coating, as described in previous studies, the approach introduced in this study is referred to as heterogeneous stripe slot coating. This work references the conventional approach illustrated in Figure 1b as "conventional stripe slot coating".

2.5. Pattern Characterization. All coating processes were carried out on a custom R2R imaging system (R2RIS). Patterned wet films were imaged in-process downstream from the coating tool outlet with a Thorlabs DCC3240C digital camera and Edmund Optics 25 mm fixed focal length lens, with an effective pixel size of 21.6 μm. Widths (w) and center-to-center distances (p) of individual stripes were extracted from these images using the MATLAB image processing toolbox.

2.6. Electrical Characterization. Resistance was measured using a Keithley 2401 source meter and a 4-contact probe. The probe contacts are line elements of polished copper, with 2.31 mm center-to-center spacing and 25.5 μm width. Prior to each measurement, patterned films were lifted from the PET substrate using scotch tape, in order to expose a pristine surface for contact with the electrical probe. Film stripes were then oriented perpendicular to the probe line contacts. Measurements taken with this setup represent the effective resistance along a 2.29 mm length of stripe; resistivity was calculated from these resistance values and the physical dimensions (thickness and width) of the patterned film.

2.7. Cross-Section Analysis. Film samples were backed with electrically conductive aluminum tape (3M 1170) and mounted in acrylic mold compound, CASTAMOUNT from PACE Technologies. The mounted samples were faced with an end mill to expose a pristine cross-section for imaging. Optical imaging was carried out on a Leica DVM6 digital microscope, and film thickness of the cross-section at PEDOT:PSS-rich regions was extracted from image data.

3. RESULTS AND DISCUSSION

3.1. Process Performance. *3.1.1. Process Sensitivity.* The sensitivity of pattern morphology to the processing conditions used for heterogeneous stripe slot coating is considered first. As a basis for comparison, the slot coating of PVA in narrow stripes with no second liquid phase, which follows the conventional approach, is also characterized. A comparison of pattern morphology as a function of process conditions for each of these cases is shown in Figure 2 using the process parameters illustrated schematically in Figure 1a. Here, coated stripe width (w) normalized by the outlet width (w_0) provides a quantitative measure of the pattern output. In agreement with previous studies,[59,79] Figure 2a shows how pattern output is strongly influenced both by the fluid volume deposited per unit of substrate (Q/V) and the coating gap between the coating tool and substrate (H). Because average wet film thickness (t_{avg}) is given by $t_{avg} = Q/(V{\cdot}w)$, process characterization over a range of Q, V, and H is effectively a requirement for simultaneous control over both stripe width and film thickness. By contrast, the introduction of a second fluid phase reduces the sensitivity of w to these process inputs considerably, as illustrated in Figure 2b. Thus, desired average wet film thickness can be specified in the same manner as the conventional approach, while the pattern morphology is determined independently by the coating tool geometry and the ratio between flow rates of the two fluid species. This constitutes a significant advantage for the heterogeneous stripe slot-coating technique.

3.1.2. Wetting of Heterogeneous Film on PET Substrate. The compatibility of the heterogeneous stripe slot-coating approach with undoped aqueous PEDOT:PSS solution stands in contrast to the conventional slot-coating approach, where surfactants or other additives are needed to prevent dewetting after deposition.[26,84,85] To investigate the favorable wetting behavior observed in alternating stripes of PEDOT:PSS and PVA, results from goniometry measurements of various

https://dx.doi.org/10.1021/acsami.9b18936
ACS Appl. Mater. Interfaces 2020, 12, 3736−3745

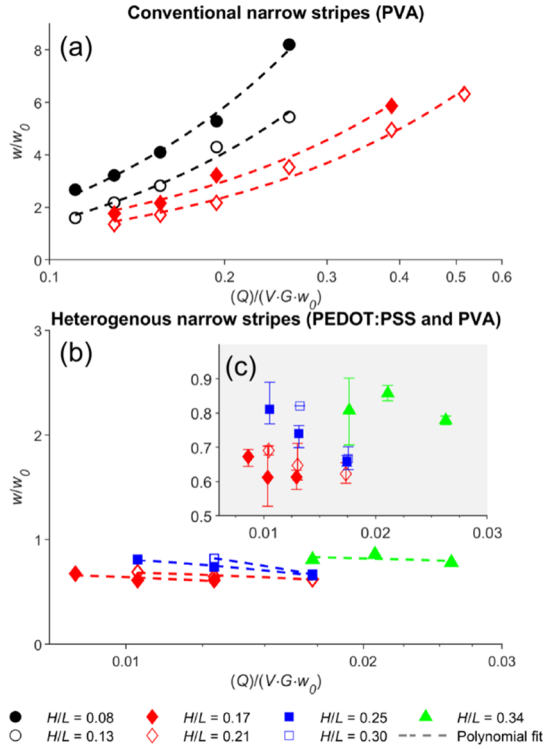

Figure 2. Pattern morphology of the wet film measured in-process across a range of Q, V, and H for (a) the conventional stripe slot-coating approach and (b) the heterogeneous stripe slot-coating approach. Outlet width w_0 is set to 1.4 and 0.94 mm in (a,b), respectively. The inset (c) presents the heterogeneous stripe coating results with different vertical axis scaling, in order to resolve closely spaced data points.

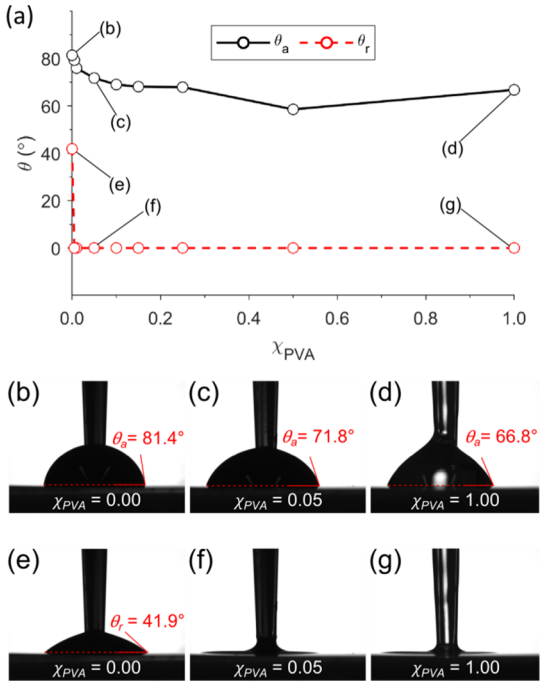

Figure 3. (a) Advancing and receding contact angles of PEDOT:PSS/PVA mixtures ranging from various volume fraction of PVA (χ_{PVA}), where $\chi_{PVA} = 0$ denotes as-received PEDOT:PSS solution and $\chi_{PVA} = 1$ denotes 10 wt % aqueous PVA. Where pinning of the contact line is observed, θ_r is recorded as 0. For $\chi_{PVA} = 1$, $\chi_{PVA} = 0.05$, and $\chi_{PVA} = 0$, advancing contact angle images are shown in (b–d), and receding contact angles are shown in (e–g).

mixtures of the two fluids on the PET substrate are shown in Figure 3. In Figure 3a, pinning of the contact line is observed for every mixture considered, even with as little as 0.5 wt % PVA. Similarly, the advancing contact angle varies by about 9.6° over the range of mixtures containing less than 5 wt % PVA, and only another 5° over the range of mixtures containing 5 wt % PVA or more. These results suggest the PVA itself acts as a wetting-enhancing dopant for PEDOT:PSS at heterogeneous liquid phase boundaries. It may also be the case that PVA acts as a scaffold for the PEDOT:PSS stripes and that diffusion-driven mixing between the two fluids is sufficiently slow to ensure stability of the pattern before curing. This would help explain why the alternating-stripe patterns remain stable even in cases with high PEDOT:PSS volume loading, which contain significant regions of PVA-free wet film.

3.2. Film Structure and Properties. *3.2.1. Feature Size and Morphology.* Using the heterogeneous stripe slot coating approach, the volume loading ratio between two coating fluids can be varied to produce a range of feature sizes with fixed tool geometry. Figure 4 illustrates the influence of $Q_{PEDOT:PSS}/Q_{PVA}$, the volume loading ratio between PEDOT:PSS and PVA, on the morphology of the resulting heterogeneous film. Microscopy images of individual stripes, shown in Figure 4a,b, exhibit gradated interphase regions containing a blend of PEDOT:PSS and PVA, roughly 200–300 μm across, and constituting the majority of total stripe width (w). Regions of concentrated PEDOT:PSS are apparent along the centerlines of stripes and at the lateral edges of the entire film, especially at higher PEDOT:PSS loading. Figure 4c plots the response of w and center-to-center spacing (p) as a function of $Q_{PEDOT:PSS}/Q_{PVA}$. Here, w is more process-sensitive, whereas p is largely determined by the geometry of the coating tool. The slight decrease in p with increasing PEDOT:PSS loading corresponds to a wetting-driven redistribution of conductive ink toward the lateral edges of the film, which can be seen in Figure 4a,b. Similarly, w is somewhat sensitive to $Q_{PEDOT:PSS}/Q_{PVA}$ but not proportional. For example, the film samples shown in Figure 4a,b represent a roughly 5% increase in stripe width due to a 100% increase in PEDOT:PSS loading. The major difference between the two samples is the region of concentrated PEDOT:PSS at the stripe center, rather than the overall stripe width. This indicates that for the conditions used in this study, w is defined largely by the passive mixing processes that produce the gradated interphase region. Furthermore, with increasing PEDOT:PSS loading, the majority of additional conductive ink is distributed to the central regions of stripes, as well as the lateral edges of the heterogeneous film.

3.2.2. Functional Properties. The electrical performance of dry heterogeneous narrow-stripe films across a range of feature sizes is presented in Figure 5. These results compare favorably with previously reported values for undoped PEDOT:PSS in the range of 1 S cm^{-1} or lower.[51,85,93−96,101] In Figure 5a, electrical conductivity (σ) correlates positively with PEDOT:PSS loading relative to PVA ($Q_{PEDOT:PSS}/Q_{PVA}$). The empirical trend appears roughly linear at $Q_{PEDOT:PSS}/Q_{PVA}$ less than 1.5 and begins to level off toward 1.5 S cm^{-1} thereafter. The overall trend in Figure 5a reflects the direct correlation between conductance and PEDOT:PSS loading across the entire film, and the diminishing sensitivity of this correlation at higher $Q_{PEDOT:PSS}/Q_{PVA}$ can be explained by the redistribution

https://dx.doi.org/10.1021/acsami.9b18936
ACS Appl. Mater. Interfaces 2020, 12, 3736−3745

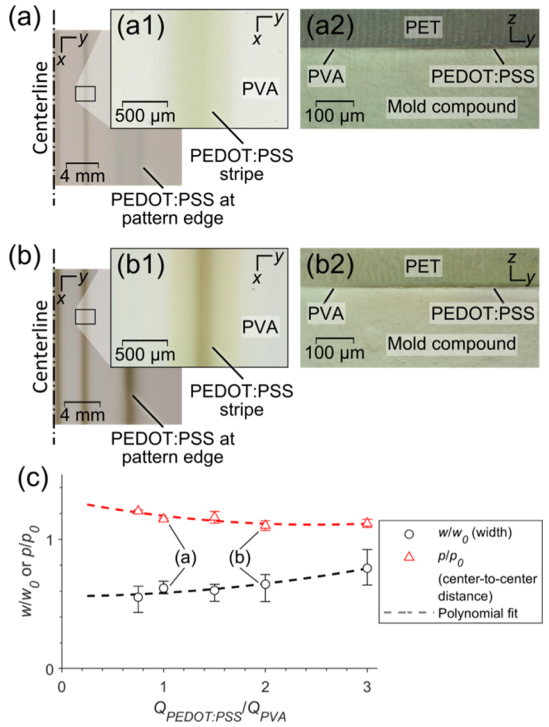

Figure 4. Optical microscopy of dry films for (a) $Q_{PEDOT:PSS}/Q_{PVA}$ = 1.0 and (b) $Q_{PEDOT:PSS}/Q_{PVA}$ = 2.0, with redistribution of PEDOT:PSS to the lateral edges of the pattern indicated. Individual stripes from (a,b) are shown from top in (a1,b1), respectively. Cross-sectional images of PEDOT:PSS/PVA interphase regions from (a,b) are shown in (a2,b2), respectively. (c) Pattern feature size as a function of $Q_{PEDOT:PSS}/Q_{PVA}$, with process conditions corresponding (a,b) indicated. Here, w and p are normalized to outlet dimensions w_0 = 0.94 mm and p_0 = 2.9 mm, respectively, while $Q_{PEDOT:PSS}$ and Q_{PVA} represent the flow rate-per-stripe for corresponding fluid species.

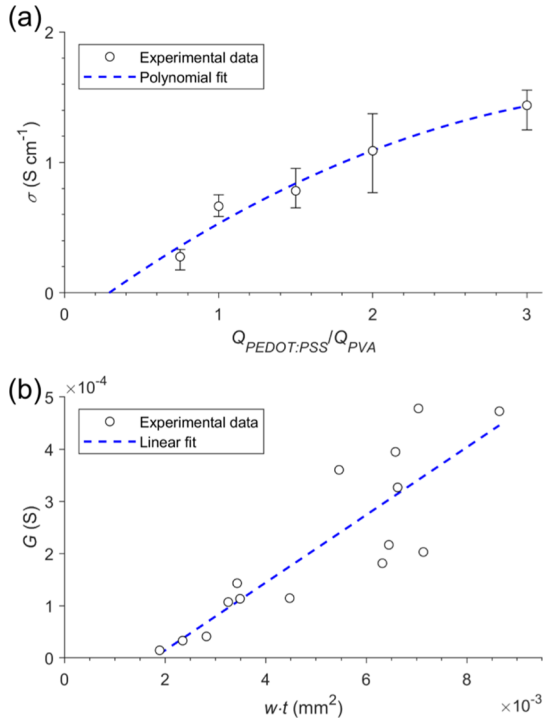

Figure 5. (a) Electrical conductivity (σ) as a function of $Q_{PEDOT:PSS}/Q_{PVA}$ for various samples. Error bars indicate the full range of variation for a given flow-rate ratio. (b) Electrical conductance (G) as a function of apparent cross-sectional area ($w{\cdot}t$) for individual printed stripes.

of PEDOT:PSS to pattern edges. The variation in conductivity at each $Q_{PEDOT:PSS}/Q_{PVA}$ value can be attributed, in part, to variations in the amount of PEDOT:PSS distributed to individual stripes, even though the total PEDOT:PSS flow rate for the entire film is pre-metered. Additionally, any transient wetting and mixing effects are likely to be exacerbated by hardware-dependent error sources such as motor vibration.

To understand these results in the context of pattern morphology, Figure 5b shows electrical conductance (G) as a function of the cross-sectional area of individual stripes ($w{\cdot}t$). The relationship between the two, which is roughly linear for the range of feature sizes produced, reflects the relative importance of the PEDOT:PSS-depleted interphase region. For stripes with large w and t, the PVA-free portion of the stripe is also large, which implies comparatively high conductance. Furthermore, extrapolation of the linear trend predicts G = 0 around $w{\cdot}t$ = 1900 μm^2. For film thicknesses in the range of 5−10 μm, this corresponds to stripe widths of 190−380 μm. Interestingly, this length scale corresponds roughly to that of the PEDOT:PSS/PVA interfaces shown in Figure 4a,b. These observations suggest a limiting feature size of roughly 400 μm, for these co-deposited materials, below which electrical performance is dominated by the PEDOT:PSS/PVA interphase.

3.2.3. Patterning Limits of Heterogeneous Stripe Slot Coating. The observed intermixing between PEDOT:PSS and PVA at stripe interfaces represents a dominant mechanism that limits the feature size of this solution pair when using the heterogeneous stripe slot-coating technique. Whereas resolution performance for the conventional slot-coating approach illustrated in Figure 1c corresponds to the length scale of the fluid menisci, which transfer coating fluid to the substrate, the feature size limitation derives from the length scale of the interphase region as determined by post-deposition intermixing. Thus, the patterning performance achieved in this work for PEDOT:PSS/PVA composite films can potentially be improved by process flow adjustments to accelerate in-line solvent removal, such as the addition of a vacuum or heating implement immediately following slot die coating. Pattern resolution may also be improved by judicious selection of the two coating fluids, such that passive mixing is minimized. However, the extreme case where both fluids are completely immiscible presents a separate limitation, which is discussed here.

Figure 6 illustrates the wetting equilibrium of two immiscible fluid materials co-deposited in alternating stripes. Here, formation of the immiscible liquid−liquid interface corresponds to significant contact line spreading and the development of a shallow sawtooth-shaped geometry. Based on common immiscible fluids at room temperature, the liquid−solid interfacial energies for both fluids A and B are assumed to be similar in magnitude ($\gamma_{S\text{-}A} \approx \gamma_{S\text{-}B}$), the surface tension of B is assumed to be greater than that of A ($\gamma_A < \gamma_B$), and the liquid−liquid interfacial tension is assumed to be significantly less than the surface tension for either A or B ($\gamma_{AB} \ll \gamma_A$, $\gamma_{AB} \ll \gamma_B$). Additionally, to preclude any Rayleigh−Taylor-type instabilities, it is also assumed that liquid B is denser than liquid A.

Static equilibrium of the pattern stricture is analyzed by Young's equation for wetting and spreading.[102] Conventional

https://dx.doi.org/10.1021/acsami.9b18936
ACS Appl. Mater. Interfaces 2020, 12, 3736−3745

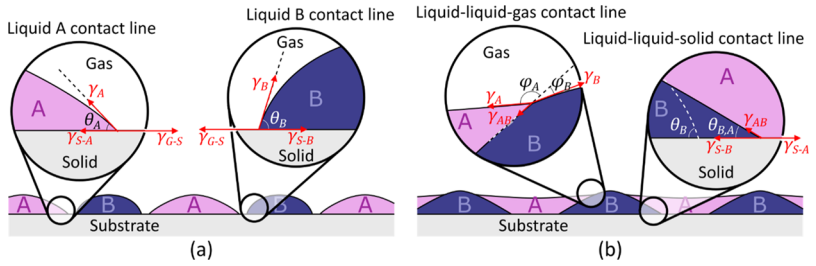

Figure 6. Schematic of macro-scale wetting equilibrium of alternating stripes of two immiscible materials, for the scenarios where (a) the liquid phases remain separate and (b) the liquid phases interact to form a liquid−liquid interface. Surface tension of liquid phases A and B are denoted as γ_A and γ_B, respectively, and γ_{AB} is the interfacial tension between A and B. The surface energy of the substrate in atmosphere, in liquid A and in liquid B, is denoted as γ_{G-S}, γ_{S-A}, and γ_{S-B}, respectively.

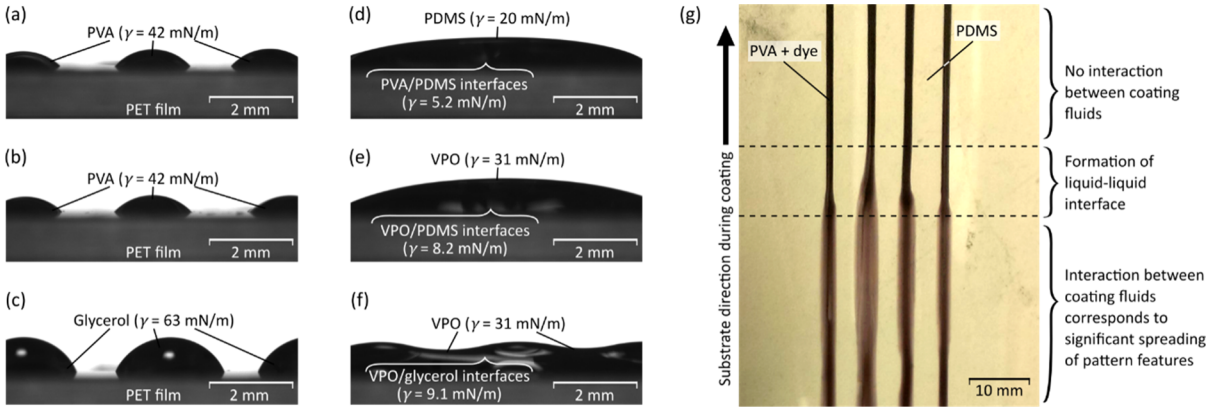

Figure 7. Wetting behavior of heterogeneous narrow-stripe films structures comprising two immiscible liquids. Profile views of the film structure for three immiscible fluid pairs (a−c) with only the denser of the two fluid species deposited in narrow stripes, and (d−f) after deposition of the second fluid species. (g) Onset of severe spreading in a PVA/PDMS narrow stripe pattern due to formation of the liquid−liquid interface.

stripe slot coating, where each liquid species is deposited separately, corresponds to the case illustrated in Figure 6a. Here, the two liquid phases do not interact, and static equilibrium is given by

$$\gamma_{G-S} = \gamma_A + \gamma_A \cos \theta_A \quad (1a)$$

$$\gamma_{G-S} = \gamma_B + \gamma_B \cos \theta_B \quad (1b)$$

where γ_{G-S} is the gas−solid interfacial energy, γ_{S-A} and γ_{S-B} are liquid−solid interfacial energies, γ_A and γ_B are surface tension values, and A and B subscripts denote liquid species. Heterogeneous stripe slot coating, as illustrated in Figure 6b, implies the formation of a liquid−liquid interface, a liquid−liquid−gas contact line, and a liquid−liquid−solid contact line. At the liquid−liquid−solid contact line, static equilibrium is given by

$$0 = \gamma_{S-B} - \gamma_{S-A} + \gamma_{AB} \cos \theta_{B,A} \quad (2)$$

where γ_{AB} is the liquid−liquid interfacial energy and $\theta_{B,A}$ is the contact angle of fluid species B with A as the outer phase. Given the relatively small magnitude of γ_{AB}, the contact angle of liquid phase B must adjust to a significantly smaller value than the case illustrated in Figure 6a. Because the liquid regions are finite in volume, this corresponds to spreading of B into A along the substrate. At the liquid−liquid−gas contact line, static equilibrium is illustrated in Figure 6b and given by

$$0 = \gamma_{AB} - \gamma_A \cos \varphi_A + \gamma_B \cos \varphi_B \quad (3a)$$

$$0 = \gamma_A \sin \varphi_A - \gamma_B \sin \varphi_B \quad (3b)$$

where φ_A and φ_B denote contact angles at the liquid−liquid−gas contact. Here, the small value of γ_{AB} relative to both γ_A and γ_B produces a significant difference in contact angles for the two fluid species, corresponding to a preferential wetting of A along the surface of B.

Demonstrations of the predicted wetting equilibrium for three separate immiscible fluid pairs are visualized Figure 7. For these demonstrations, an initial fluid phase, either PVA prepared in 24 wt % aqueous solution or glycerol prepared in 95 wt % solution, is deposited by a syringe dispenser in narrow stripes on PET substrate, as shown in Figure 7a−c. Subsequently, a second fluid phase corresponding to liquid B in Figure 7d−f, either PDMS or VPO, is deposited. The wetting properties of these fluids encompass a representative range for room-temperature coating fluids. Surface tension of PVA, glycerol, PDMS, and VPO are 42, 63, 20, and 31 mN m^{-1}, respectively. The PVA and glycerol concentrations ensure relatively high viscosities (1057 and 346 cP, respectively) to facilitate deposition of high aspect ratio stripes but otherwise have no significance to the equilibrium film structure. Additionally, the interfacial tension between PVA and PDMS, PVA and VPO, and glycerol and VPO are 5.1, 8.2, and 9.1 mN m^{-1}, respectively.

Comparing the single-fluid structures in Figure 7a−c to the two-fluid structures in Figure 7d−f, spreading of fluid phase A along B predicted by the equilibrium wetting analysis is evident. The significance of this wetting regime to the heterogeneous slot-coating process is illustrated in Figure 7g with alternating narrow-stripe regions of PVA and PDMS. Here, less than 1% dye has been added to the PVA for

https://dx.doi.org/10.1021/acsami.9b18936
ACS Appl. Mater. Interfaces 2020, 12, 3736−3745

visualization purposes. While relatively narrow stripes of each material are deposited through single-material liquid bridges, the onset of their interaction shown in the center section of Figure 7g corresponds to sudden and significant apparent spreading in the pattern, seen in the lower section of the image.

The wetting behavior illustrated in Figures 6 and 7 constitutes a significant consideration for material selection in heterogeneous stripe slot coating. Whereas the codeposition of miscible PEDOT:PSS and PVA facilitates control over pattern morphology, codeposition of immiscible fluid pairs is subject to coupling between the stripe width and film thickness. Furthermore, the feature size of the sawtooth-like equilibrium structure illustrated in Figure 6b is categorically poor compared to free-standing homogeneous stripes. Thus, optimization of feature size performance must balance the need for miscibility between co-deposited fluid materials against potential loss in pattern fidelity due to intermixing. Notably, the intermixed region may not be undesirable in every case. Devices and material systems where the interphase region provides distinct functionality, such as bulk heterojunction and graded heterojunction semiconductor devices,[103−107] may derive unique benefits from the slot-coating approach developed in this work.

4. CONCLUSIONS

This investigation has demonstrated R2R deposition of undoped PEDOT:PSS in 400−850 μm-wide stripes, using a novel technique inspired by slot die coating. This approach circumvents the need for pattern masks, selective wettability enhancements to the substrate, and compensation for wetting and spreading effects at pattern feature edges required by other recently proposed patterning techniques. Furthermore, the technique described in this work eliminates the wettability-enhancing additive requirement previously described for PEDOT:PSS inks deposited on untreated plastic substrate. After thermal annealing, PEDOT:PSS stripes from this work exhibit electrical conductivity in excess of 1.5 S cm^{-1}, among the highest reported values for PEDOT:PSS prior to standard acid post-treatments. The sheet resistance of these patterned films decreases exponentially with the stripe width, and inspection of the interphase region between PEDOT:PSS and PVA suggests that at feature sizes below 400 μm, film properties are dominated by the interphase region, rather than the central region of high PEDOT:PSS concentration.

The heterogeneous stripe slot-coating approach is readily applicable across various devices including sensors, thin film transistors, optical filters, and microfluidic devices, which have previously been demonstrated in architectures incorporating stripe-patterned composite films of two or more materials. Furthermore, the diffuse PEDOT:PSS/PVA interphase regions observed in samples fabricated for the present investigation suggest a potential benefit for devices where the interphase region provides distinct functionality. For this purpose, further investigations on postdeposition diffusive mixing will be useful for optimizing the functional performance of heterogeneous narrow-stripe films. The mixing-related feature size limitations highlighted in this work may potentially be overcome by process modifications to accelerate postdeposition curing. Similarly, it may be possible to overcome the fluid interface-mediated feature size limitation for immiscible materials highlighted in this work by increasing coating fluid viscosity or by introducing a favorable surface tension gradient across the two co-deposited fluids. The decoupling of pattern morphology from average film thickness, together with minimal wettability-driven material restrictions, suggests that the processing method from this study may be extended to a wide range of inks and coating materials.

AUTHOR INFORMATION

Corresponding Author

Tequila A. L. Harris − *Georgia Institute of Technology, Atlanta, Georgia;* orcid.org/0000-0002-6086-6987; Phone: (404) 385-6335; Email: tequila.harris@me.gatech.edu; Fax: (404) 894-9342

Other Author

Ara W. Parsekian − *Georgia Institute of Technology, Atlanta, Georgia*

Complete contact information is available at: https://pubs.acs.org/10.1021/acsami.9b18936

Notes

The authors declare no competing financial interest.

ACKNOWLEDGMENTS

This work was supported by the National Science Foundation under grant no. 1069138, CMMI MEP-1562255. Measurements of liquid−liquid interfacial tension were performed by Ana Girardot. The authors would also like to thank Dr. Suresh Sitaraman for use of his electrical characterization facilities and the Georgia Tech Materials Innovation and Learning Laboratory for use of their Leica DVM6 optical microscope. Finally, the authors would like to acknowledge Dr. Lorraine Francis for her invaluable insights and feedback.

ABBREVIATIONS

PDMS, polydimethylsiloxane
PEDOT:PSS, poly(3,4-ethylenedioxythiophene):polystyrene sulfonate
PET, poly(ethylene terephthalate)
PTFE, polytetrafluoroethylene
PVA, polyvinyl alcohol
R2R, roll-to-roll
R2RIS, roll-to-roll imaging system
VPO, vacuum pump oil

REFERENCES

(1) Gustafsson, G.; Cao, Y.; Treacy, G. M.; Klavetter, F.; Colaneri, N.; Heeger, A. J. Flexible Light-Emitting Diodes Made from Soluble Conducting Polymers. *Nature* **1992**, *357*, 477−479.
(2) Service, R. F. Patterning Electronics on the Cheap. *Science* **1997**, *278*, 383−384.
(3) Derby, B. Inkjet Printing of Functional and Structural Materials: Fluid Property Requirements, Feature Stability, and Resolution. *Annu. Rev. Mater. Res.* **2010**, *40*, 395−414.
(4) Søndergaard, R. R.; Hösel, M.; Krebs, F. C. Roll-to-Roll Fabrication of Large Area Functional Organic Materials. *J. Polym. Sci., Part B: Polym. Phys.* **2013**, *51*, 16−34.
(5) Khan, S.; Lorenzelli, L.; Dahiya, R. S. Technologies for Printing Sensors and Electronics over Large Flexible Substrates: A Review. *IEEE Sens. J.* **2015**, *15*, 3164−3185.
(6) Bhamidipati, K. L.; Didari, S.; Bedell, P.; Harris, T. A. L. Wetting Phenomena During Processing of High-Viscosity Shear-Thinning Fluid. *J. Non-Newtonian Fluid Mech.* **2011**, *166*, 723−733.
(7) Kumar, S. Liquid Transfer in Printing Processes: Liquid Bridges with Moving Contact Lines. *Annu. Rev. Fluid. Mech.* **2015**, *47*, 67−94.

(8) Kalpathy, S. K.; Francis, L. F.; Kumar, S. Thin-Film Models of Liquid Displacement on Chemically Patterned Surfaces for Lithographic Printing Processes. *J. Colloid Interface Sci.* **2012**, *383*, 155−166.
(9) Etxebarria, I.; Tait, J. G.; Gehlhaar, R.; Pacios, R.; Cheyns, D. Surface Treatment Patterning of Organic Photovoltaic Films for Low-Cost Modules. *Org. Electron.* **2013**, *14*, 430−435.
(10) Efremov, A. N.; Grunze, M.; Levkin, P. A. Digital Liquid Patterning: A Versatile Method for Maskless Generation of Liquid Patterns and Gradients. *Adv. Mater. Interfaces* **2014**, *1*, 1300075.
(11) Harirchian-Saei, S.; Wang, M. C. P.; Gates, B. D.; Moffitt, M. G. Patterning Block Copolymer Aggregates Via Langmuir−Blodgett Transfer to Microcontact-Printed Substrates. *Langmuir* **2010**, *26*, 5998−6008.
(12) Harirchian-Saei, S.; Wang, M. C. P.; Gates, B. D.; Moffitt, M. G. Simultaneous Patterning of Two Different Types of Nanoparticles into Alternating Domains of a Striped Array of a Polymer Blend in a Single Spin-Casting Step. *J. Colloid Interface Sci.* **2014**, *433*, 123−132.
(13) Tehrani, P.; Robinson, N. D.; Kugler, T.; Remonen, T.; Hennerdal, L.-O.; Häll, J.; Malmström, A.; Leenders, L.; Berggren, M. Patterning Polythiophene Films Using Electrochemical over-Oxidation. *Smart Mater. Struct.* **2005**, *14*, N21.
(14) Ikenoue, T.; Kameyama, N.; Fujita, S. Fabrication of PEDOT:PSS/ZnMgO Schottky-Type Ultraviolet Sensors on Glass Substrates with Solution-Based Mist Deposition Technique and Hard-Mask Patterning. *Phys. Status Solidi C* **2011**, *8*, 613−615.
(15) Charlot, B.; Sassine, G.; Garraud, A.; Sorli, B.; Giani, A.; Combette, P. Micropatterning PEDOT:PSS Layers. *Microsyst. Technol.* **2013**, *19*, 895−903.
(16) Sun, J.; Chen, C.; Song, J.; Liu, J.; Yang, X.; Liu, J.; Liu, X.; Lu, Y. A Universal Method to Create Surface Patterns with Extreme Wettability on Metal Substrates. *J. Colloid Interface Sci.* **2019**, *535*, 100−110.
(17) Huiskamp, T.; Brok, W. J. M.; Stevens, A. A. E.; van Heesch, E. J. M.; Pemen, A. J. M. Maskless Patterning by Pulsed-Power Plasma Printing. *IEEE Trans. Plasma Sci.* **2012**, *40*, 1913−1925.
(18) Kubis, P.; Lucera, L.; Machui, F.; Spyropoulos, G.; Cordero, J.; Frey, A.; Kaschta, J.; Voigt, M. M.; Matt, G. J.; Zeira, E.; Brabec, C. J. High Precision Processing of Flexible P3HT/PCBM Modules with Geometric Fill Factor over 95%. *Org. Electron.* **2014**, *15*, 2256−2263.
(19) Friedrich, M.; Gibson, G. Methods for Minimizing Slot Die Coating Edge Effects and Patterned Coating. In *18th International Coating Science and Technology Symposium, Pittsburgh, PA*, 2016.
(20) Diao, Y.; Shaw, L.; Bao, Z.; Mannsfeld, S. C. B. Morphology Control Strategies for Solution-Processed Organic Semiconductor Thin Films. *Energy Environ. Sci.* **2014**, *7*, 2145−2159.
(21) Wang, F.; Cao, Y.; Chen, C.; Chen, Q.; Wu, X.; Li, X.; Qin, T.; Huang, W. Materials toward the Upscaling of Perovskite Solar Cells: Progress, Challenges, and Strategies. *Adv. Funct. Mater.* **2018**, *28*, 1803753.
(22) Richard, M.; Al-Ajaji, A.; Ren, S.; Foti, A.; Tran, J.; Frigoli, M.; Gusarov, B.; Bonnassieux, Y.; Caurel, E. G.; Bulkin, P.; Ossikovski, R.; Yassar, A. Large-Scale Patterning of Π-Conjugated Materials by Meniscus Guided Coating Methods. *Adv. Colloid Interface Sci.* **2020**, *275*, 102080.
(23) Kwak, M. K.; Shin, K. H.; Yoon, E. Y.; Suh, K. Y. Fabrication of Conductive Metal Lines by Plate-to-Roll Pattern Transfer Utilizing Edge Dewetting and Flexographic Printing. *J. Colloid Interface Sci.* **2010**, *343*, 301−305.
(24) Iannaccone, G.; Välimäki, M.; Jansson, E.; Sunnari, A.; Corso, G.; Bernardi, A.; Levi, M.; Turri, S.; Hast, J.; Griffini, G. Roll-to-Roll Compatible Flexible Polymer Solar Cells Incorporating a Water-Based Solution-Processable Silver Back Electrode with Low Annealing Temperature. *Sol. Energy Mater. Sol. Cells* **2015**, *143*, 227−235.
(25) Andersen, T. R.; Cooling, N. A.; Almyahi, F.; Hart, A. S.; Nicolaidis, N. C.; Feron, K.; Noori, M.; Vaughan, B.; Griffith, M. J.; Belcher, W. J.; Dastoor, P. C. Fully Roll-to-Roll Prepared Organic Solar Cells in Normal Geometry with a Sputter-Coated Aluminium Top-Electrode. *Sol. Energy Mater. Sol. Cells* **2016**, *149*, 103−109.
(26) Voigt, M. M.; Mackenzie, R. C. I.; Yau, C. P.; Atienzar, P.; Dane, J.; Keivanidis, P. E.; Bradley, D. D. C.; Nelson, J. Gravure Printing for Three Subsequent Solar Cell Layers of Inverted Structures on Flexible Substrates. *Sol. Energy Mater. Sol. Cells* **2011**, *95*, 731−734.
(27) Park, K.; Woo, K.; Kim, J.; Lee, D.; Ahn, Y.; Song, D.; Kim, H.; Oh, D.; Kwon, S.; Lee, Y. High-Resolution and Large-Area Patterning of Highly Conductive Silver Nanowire Electrodes by Reverse Offset Printing and Intense Pulsed Light Irradiation. *ACS Appl. Mater. Interfaces* **2019**, *11*, 14882−14891.
(28) Liang, J.; Tong, K.; Pei, Q. A Water-Based Silver-Nanowire Screen-Print Ink for the Fabrication of Stretchable Conductors and Wearable Thin-Film Transistors. *Adv. Mater.* **2016**, *28*, 5986−5996.
(29) Ibáñez-Redín, G.; Wilson, D.; Gonçalves, D.; Oliveira, O. N. Low-Cost Screen-Printed Electrodes Based on Electrochemically Reduced Graphene Oxide-Carbon Black Nanocomposites for Dopamine, Epinephrine and Paracetamol Detection. *J. Colloid Interface Sci.* **2018**, *515*, 101−108.
(30) Pali, L. S.; Jindal, R.; Garg, A. Screen Printed Pedot:Pss Films as Transparent Electrode and Its Application in Organic Solar Cells on Opaque Substrates. *J. Mater. Sci.: Mater. Electron.* **2018**, *29*, 11030−11038.
(31) Calvert, P. Inkjet Printing for Materials and Devices. *Chem. Mater.* **2001**, *13*, 3299−3305.
(32) de Gans, B.-J.; Duineveld, P. C.; Schubert, U. S. Inkjet Printing of Polymers: State of the Art and Future Developments. *Adv. Mater.* **2004**, *16*, 203−213.
(33) Stringer, J.; Derby, B. Formation and Stability of Lines Produced by Inkjet Printing. *Langmuir* **2010**, *26*, 10365−10372.
(34) Singh, M.; Haverinen, H. M.; Dhagat, P.; Jabbour, G. E. Inkjet Printing—Process and Its Applications. *Adv. Mater.* **2010**, *22*, 673−685.
(35) Liu, H.; Xu, W.; Tan, W.; Zhu, X.; Wang, J.; Peng, J.; Cao, Y. Line Printing Solution-Processable Small Molecules with Uniform Surface Profile Via Ink-Jet Printer. *J. Colloid Interface Sci.* **2016**, *465*, 106−111.
(36) Shahariar, H.; Kim, I.; Soewardiman, H.; Jur, J. S. Inkjet Printing of Reactive Silver Ink on Textiles. *ACS Appl. Mater. Interfaces* **2019**, *11*, 6208−6216.
(37) Soltman, D.; Smith, B.; Kang, H.; Morris, S. J. S.; Subramanian, V. Methodology for Inkjet Printing of Partially Wetting Films. *Langmuir* **2010**, *26*, 15686−15693.
(38) Soltman, D.; Smith, B.; Morris, S. J. S.; Subramanian, V. Inkjet Printing of Precisely Defined Features Using Contact-Angle Hysteresis. *J. Colloid Interface Sci.* **2013**, *400*, 135−139.
(39) Chang, C.-J.; Lin, Y.-H.; Tsai, H.-Y. Synthesis and Properties of Uv-Curable Hyperbranched Polymers for Ink-Jet Printing of Color Micropatterns on Glass. *Thin Solid Films* **2011**, *519*, 5243−5248.
(40) Radha, B.; Sagade, A. A.; Kulkarni, G. U. Flexible and Semitransparent Strain Sensors Based on Micromolded Pd Nanoparticle−Carbon M-Stripes. *ACS Appl. Mater. Interfaces* **2011**, *3*, 2173−2178.
(41) Ueno, S.; Taguchi, Y.; Saeki, K.; Okada, M.; Nagino, S.; Hashimoto, K.; Tachikawa, T. A New Wettability-Control Technique for Fabricating Color Oled Panels by an Ink-Jet-Printing Method. *J. Soc. Inf. Disp.* **2011**, *19*, 87−93.
(42) Ko, H.; Lee, J.; Kim, Y.; Lee, B.; Jung, C.-H.; Choi, J.-H.; Kwon, O.-S.; Shin, K. Active Digital Microfluidic Paper Chips with Inkjet-Printed Patterned Electrodes. *Adv. Mater.* **2014**, *26*, 2335−2340.
(43) Tang, W.; Feng, L.; Zhao, J.; Cui, Q.; Chen, S.; Guo, X. Inkjet Printed Fine Silver Electrodes for All-Solution-Processed Low-Voltage Organic Thin Film Transistors. *J. Mater. Chem. C* **2014**, *2*, 1995−2000.
(44) Seifert, T.; Sowade, E.; Roscher, F.; Wiemer, M.; Gessner, T.; Baumann, R. R. Additive Manufacturing Technologies Compared: Morphology of Deposits of Silver Ink Using Inkjet and Aerosol Jet Printing. *Ind. Eng. Chem. Res.* **2015**, *54*, 769−779.

https://dx.doi.org/10.1021/acsami.9b18936
ACS Appl. Mater. Interfaces 2020, 12, 3736−3745

(45) Rahman, M. T.; Rahimi, A.; Gupta, S.; Panat, R. Microscale Additive Manufacturing and Modeling of Interdigitated Capacitive Touch Sensors. *Sens. Actuators, A* **2016**, *248*, 94−103.
(46) Jin Lee, S.; Kim, Y.-J.; Young Yeo, S.; Lee, E.; Sun Lim, H.; Kim, M.; Song, Y.-W.; Cho, J.; Ah Lim, J. Centro-Apical Self-Organization of Organic Semiconductors in a Line-Printed Organic Semiconductor: Polymer Blend for One-Step Printing Fabrication of Organic Field-Effect Transistors. *Sci. Rep.* **2015**, *5*, 14010.
(47) Friedrich, L.; Begley, M. In Situ Characterization of Low-Viscosity Direct Ink Writing: Stability, Wetting, and Rotational Flows. *J. Colloid Interface Sci.* **2018**, *529*, 599−609.
(48) Alizadehgiashi, M.; Gevorkian, A.; Tebbe, M.; Seo, M.; Prince, E.; Kumacheva, E. 3d-Printed Microfluidic Devices for Materials Science. *Adv. Mater. Technol.* **2018**, *3*, 1800068.
(49) Chen, C.-Y.; Chang, H.-W.; Chang, Y.-F.; Chang, B.-J.; Lin, Y.-S.; Jian, P.-S.; Yeh, H.-C.; Chien, H.-T.; Chen, E.-C.; Chao, Y.-C.; Meng, H.-F.; Zan, H.-W.; Lin, H.-W.; Horng, S.-F.; Cheng, Y.-J.; Yen, F.-W.; Lin, I.-F.; Yang, H.-Y.; Huang, K.-J.; Tseng, M.-R. Continuous Blade Coating for Multi-Layer Large-Area Organic Light-Emitting Diode and Solar Cell. *J. Appl. Phys.* **2011**, *110*, 094501.
(50) Eric Shen, D.; Österholm, A. M.; Reynolds, J. R. Out of Sight but Not out of Mind: The Role of Counter Electrodes in Polymer-Based Solid-State Electrochromic Devices. *J. Mater. Chem. C* **2015**, *3*, 9715−9725.
(51) De Keersmaecker, M.; Lang, A. W.; Österholm, A. M.; Reynolds, J. R. All Polymer Solution Processed Electrochromic Devices: A Future without Indium Tin Oxide? *ACS Appl. Mater. Interfaces* **2018**, *10*, 31568−31579.
(52) Mao, C.; Huang, J.; Zhu, Y.; Jiang, W.; Tang, Q.; Ma, X. Tailored Parallel Graphene Stripes in Plastic Film with Conductive Anisotropy by Shear-Induced Self-Assembly. *J. Phys. Chem. Lett.* **2013**, *4*, 43−47.
(53) Huang, J.; Zhu, Y.; Jiang, W.; Tang, Q. Parallel Carbon Nanotube Stripes in Polymer Thin Film with Tunable Microstructures and Anisotropic Conductive Properties. *Composites, Part A* **2015**, *69*, 240−246.
(54) Becerril, H. A.; Roberts, M. E.; Liu, Z.; Locklin, J.; Bao, Z. High-Performance Organic Thin-Film Transistors through Solution-Sheared Deposition of Small-Molecule Organic Semiconductors. *Adv. Mater.* **2008**, *20*, 2588−2594.
(55) Yabu, H.; Shimomura, M. Preparation of Self-Organized Mesoscale Polymer Patterns on a Solid Substrate: Continuous Pattern Formation from a Receding Meniscus. *Adv. Funct. Mater.* **2005**, *15*, 575−581.
(56) Brabec, C. J.; Durrant, J. R. Solution-Processed Organic Solar Cells. *MRS Bull.* **2008**, *33*, 670−675.
(57) Wen, S.-H.; Liu, T.-J. Extrusion Die Design for Multiple Stripes. *Polym. Eng. Sci.* **1995**, *35*, 759−767.
(58) Hösel, M.; Søndergaard, R. R.; Jørgensen, M.; Krebs, F. C. Fast Inline Roll-to-Roll Printing for Indium-Tin-Oxide-Free Polymer Solar Cells Using Automatic Registration. *Energy Technol.* **2013**, *1*, 102−107.
(59) Lin, C.-F.; Wang, B.-K.; Lo, S.-H.; Wong, D. S.-H.; Liu, T.-J.; Tiu, C. Operating Windows of Stripe Coating. *Asia-Pac. J. Chem. Eng.* **2014**, *9*, 134−145.
(60) Schmitt, M.; Scharfer, P.; Schabel, W. Slot Die Coating of Lithium-Ion Battery Electrodes: Investigations on Edge Effect Issues for Stripe and Pattern Coatings. *J. Coat. Technol. Res.* **2014**, *11*, 57−63.
(61) Raupp, S. M.; Schmitt, M.; Walz, A.-L.; Diehm, R.; Hummel, H.; Scharfer, P.; Schabel, W. Slot Die Stripe Coating of Low Viscous Fluids. *J. Coat. Technol. Res.* **2018**, *15*, 899−911.
(62) Kutsarov, D. I.; New, E.; Bausi, F.; Zoladek-Lemanczyk, A.; Castro, F. A.; Silva, S. R. P. Fabrication of Air-Stable, Large-Area, Pcdtbt:Pc70bm Polymer Solar Cell Modules Using a Custom Built Slot-Die Coater. *Sol. Energy Mater. Sol. Cells* **2017**, *161*, 388−396.
(63) Vak, D.; Hwang, K.; Faulks, A.; Jung, Y.-S.; Clark, N.; Kim, D.-Y.; Wilson, G. J.; Watkins, S. E. 3d Printer Based Slot-Die Coater as a Lab-to-Fab Translation Tool for Solution-Processed Solar Cells. *Adv. Energy Mater.* **2015**, *5*, 1401539.
(64) Chang, Y.-R.; Lin, C.-F.; Liu, T.-J. Start-up of Slot Die Coating. *Polym. Eng. Sci.* **2009**, *49*, 1158−1167.
(65) Choinski, E. J. Method and Apparatus for Patch Coating Printed Circuit Boards. U.S. Patent 4,938,994 A, July 3, 1990.
(66) Abbel, R.; de Vries, I.; Langen, A.; Kirchner, G.; t'Mannetje, H.; Gorter, H.; Wilson, J.; Groen, P. Toward High Volume Solution Based Roll-to-Roll Processing of Oleds. *J. Mater. Res.* **2017**, *32*, 2219−2229.
(67) Gu, X.; Shaw, L.; Gu, K.; Toney, M. F.; Bao, Z. The Meniscus-Guided Deposition of Semiconducting Polymers. *Nat. Commun.* **2018**, *9*, 534.
(68) Wang, G.; Adil, M. A.; Zhang, J.; Wei, Z. Large-Area Organic Solar Cells: Material Requirements, Modular Designs, and Printing Methods. *Adv. Mater.* **2019**, *31*, 1805089.
(69) Abbel, R.; Galagan, Y.; Groen, P. Roll-to-Roll Fabrication of Solution Processed Electronics. *Adv. Eng. Mater.* **2018**, *20*, 1701190.
(70) Chang, Y.-M.; Liao, C.-Y.; Lee, C.-C.; Lin, S.-Y.; Teng, N.-W.; Huei-Shuan Tan, P. All Solution and Ambient Processable Organic Photovoltaic Modules Fabricated by Slot-Die Coating and Achieved a Certified 7.56% Power Conversion Efficiency. *Sol. Energy Mater. Sol. Cells* **2019**, *202*, 110064.
(71) Zhou, G.; Li, L.; Wang, D.-W.; Shan, X.-y.; Pei, S.; Li, F.; Cheng, H.-M. A Flexible Sulfur-Graphene-Polypropylene Separator Integrated Electrode for Advanced Li−S Batteries. *Adv. Mater.* **2015**, *27*, 641−647.
(72) Sandström, A.; Dam, H. F.; Krebs, F. C.; Edman, L. Ambient Fabrication of Flexible and Large-Area Organic Light-Emitting Devices Using Slot-Die Coating. *Nat. Commun.* **2012**, *3*, 1002.
(73) Kim, G.-E.; Shin, D.-K.; Lee, J.-Y.; Park, J. Effect of Surface Morphology of Slot-Die Heads on Roll-to-Roll Coatings of Fine Pedot:Pss Stripes. *Org. Electron.* **2019**, *66*, 116−125.
(74) Choi, C.; Lin, L.; Liu, Y.; Choi, J.; Wang, L.; Haas, D.; Magera, J.; Chen, R. T. Flexible Optical Waveguide Film Fabrications and Optoelectronic Devices Integration for Fully Embedded Board-Level Optical Interconnects. *J. Lightwave Technol.* **2004**, *22*, 2168.
(75) Chang, C.-L.; Ding, Z.; Patchigolla, V. N. L. R.; Ziaie, B.; Savran, C. A. Reflective Diffraction Gratings from Hydrogels as Biochemical Sensors. *IEEE Sens. J.* **2012**, *12*, 2374−2379.
(76) Mehlich, J.; Miyata, Y.; Shinohara, H.; Ravoo, B. J. Fabrication of a Carbon-Nanotube-Based Field-Effect Transistor by Microcontact Printing. *Small* **2012**, *8*, 2258−2263.
(77) Li, Y.; Lan, L.; Xiao, P.; Sun, S.; Lin, Z.; Song, W.; Song, E.; Gao, P.; Wu, W.; Peng, J. Coffee-Ring Defined Short Channels for Inkjet-Printed Metal Oxide Thin-Film Transistors. *ACS Appl. Mater. Interfaces* **2016**, *8*, 19643−19648.
(78) Pecora, A.; Zampetti, E.; Pantalei, S.; Valletta, A.; Minotti, A.; Maiolo, L.; Simeone, D.; Cuscuna, M.; Bearzotti, A.; Macagnano, A.; Mariucci, L.; Fortunato, G. Interdigitated Sensorial System on Flexible Substrate. *Proceedings of IEEE International Conference Sensors, 7th*, 2008; pp 21−24.
(79) Parsekian, A. W.; Harris, T. A. L. Extrusion on-Demand Pattern Coating Using a Hybrid Manufacturing Process. *Chem. Eng. Process.* **2016**, *109*, 20−31.
(80) Parsekian, A. W.; Jeong, T.-J.; Harris, T. A. L. A Process Model for Slot Coating of Narrow Stripes. *J. Coat. Technol. Res.* **2019**, *16*, 1653.
(81) Parsekian, A. W.; Harris, T. A. L. *Device and Method for Scaling and Coating of Continuous Multi-Material Stripes and Patterns*. World Intellectual Property Organization, WOWO 2019109101 A1, PCT/US2018/063688, 2019.
(82) Thérien-Aubin, H.; Wu, Z. L.; Nie, Z.; Kumacheva, E. Multiple Shape Transformations of Composite Hydrogel Sheets. *J. Am. Chem. Soc.* **2013**, *135*, 4834−4839.
(83) Levermore, P. A.; Chen, L.; Wang, X.; Das, R.; Bradley, D. D. C. Fabrication of Highly Conductive Poly(3,4-Ethylenedioxythiophene) Films by Vapor Phase Polymerization and Their Application

https://dx.doi.org/10.1021/acsami.9b18936
ACS Appl. Mater. Interfaces 2020, 12, 3736−3745

in Efficient Organic Light-Emitting Diodes. *Adv. Mater.* **2007**, *19*, 2379−2385.
(84) Tvingstedt, K.; Inganäs, O. Electrode Grids for Ito Free Organic Photovoltaic Devices. *Adv. Mater.* **2007**, *19*, 2893−2897.
(85) Sun, K.; Zhang, S.; Li, P.; Xia, Y.; Zhang, X.; Du, D.; Isikgor, F. H.; Ouyang, J. Review on Application of Pedots and Pedot:Pss in Energy Conversion and Storage Devices. *J. Mater. Sci.: Mater. Electron.* **2015**, *26*, 4438−4462.
(86) Andersson, P.; Forchheimer, R.; Tehrani, P.; Berggren, M. Printable All-Organic Electrochromic Active-Matrix Displays. *Adv. Funct. Mater.* **2007**, *17*, 3074−3082.
(87) Jensen, J.; Hösel, M.; Kim, I.; Yu, J.-S.; Jo, J.; Krebs, F. C. Fast Switching Ito Free Electrochromic Devices. *Adv. Funct. Mater.* **2014**, *24*, 1228−1233.
(88) Jensen, J.; Hösel, M.; Dyer, A. L.; Krebs, F. C. Development and Manufacture of Polymer-Based Electrochromic Devices. *Adv. Funct. Mater.* **2015**, *25*, 2073−2090.
(89) Lim, F. J.; Ananthanarayanan, K.; Luther, J.; Ho, G. W. Influence of a Novel Fluorosurfactant Modified PEDOT:PSS Hole Transport Layer on the Performance of Inverted Organic Solar Cells. *J. Mater. Chem.* **2012**, *22*, 25057−25064.
(90) Vosgueritchian, M.; Lipomi, D. J.; Bao, Z. Highly Conductive and Transparent PEDOT:PSS Films with a Fluorosurfactant for Stretchable and Flexible Transparent Electrodes. *Adv. Funct. Mater.* **2012**, *22*, 421−428.
(91) Li, Z.; Meng, W.; Tong, J.; Zhao, C.; Qin, F.; Jiang, F.; Xiong, S.; Zeng, S.; Xu, L.; Hu, B.; Zhou, Y. A Nonionic Surfactant Simultaneously Enhancing Wetting Property and Electrical Conductivity of PEDOT:PSS for Vacuum-Free Organic Solar Cells. *Sol. Energy Mater. Sol. Cells* **2015**, *137*, 311−318.
(92) Cheng, T.; Zhang, Y.-Z.; Zhang, J.-D.; Lai, W.-Y.; Huang, W. High-Performance Free-Standing PEDOT:PSS Electrodes for Flexible and Transparent All-Solid-State Supercapacitors. *J. Mater. Chem. A* **2016**, *4*, 10493−10499.
(93) Li, N.; Huang, G.-W.; Xiao, H.-M.; Fu, S.-Y. Preparation of Aligned Fe3O4@Ag-Nanowire/Poly(Vinyl Alcohol) Nanocomposite Films Via a Low Magnetic Field. *Composites, Part A* **2015**, *77*, 87−95.
(94) GmbH, Clariant. *Mowiol: Polyvinyl Alcohol*; Technical Report; Clariant GmbH: Sulzbach, Hesse, Germany, 1999.
(95) Crispin, X.; Jakobsson, F. L. E.; Crispin, A.; Grim, P. C. M.; Andersson, P.; Volodin, A.; van Haesendonck, C.; Van der Auweraer, M.; Salaneck, W. R.; Berggren, M. The Origin of the High Conductivity of Poly(3,4-Ethylenedioxythiophene)−Poly-(Styrenesulfonate) (PEDOT−PSS) Plastic Electrodes. *Chem. Mater.* **2006**, *18*, 4354−4360.
(96) Friedel, B.; Keivanidis, P. E.; Brenner, T. J. K.; Abrusci, A.; McNeill, C. R.; Friend, R. H.; Greenham, N. C. Effects of Layer Thickness and Annealing of Pedot:Pss Layers in Organic Photodetectors. *Macromolecules* **2009**, *42*, 6741−6747.
(97) Xiong, Z.; Liu, C. Optimization of Inkjet Printed Pedot:Pss Thin Films through Annealing Processes. *Org. Electron.* **2012**, *13*, 1532−1540.
(98) Seki, Y.; Takahashi, M.; Takashiri, M. Enhanced Thermoelectric Properties of Electropolymerized Poly (3,4-Ethylenedioxythiophene) Thin Films by Optimizing Electrolyte Temperature and Thermal Annealing Temperature. *Org. Electron.* **2018**, *55*, 112−116.
(99) Kwon, S. W.; Yoon, D. H.; Yang, W. S. A Simple Route of Ordered High Quality Mesoscale Stripe Polymer Patterns. *Soft Matter* **2011**, *7*, 1682−1685.
(100) Yu, W.-J.; Liu, T.-J.; Yu, T.-A. Reduction of the Minimum Wet Thickness in Extrusion Slot Coating. *Chem. Eng. Sci.* **1995**, *50*, 917−920.
(101) Shi, H.; Liu, C.; Jiang, Q.; Xu, J. Effective Approaches to Improve the Electrical Conductivity of Pedot:Pss: A Review. *Adv. Electron. Mater.* **2015**, *1*, 1500017.
(102) Rowlinson, J. S.; Widom, B. Three-Phase Equilibrium. In *Molecular Theory of Capillarity*, 2002 ed.; Dover Publications: Mineloa, NY, 2002; pp 209−212.
(103) Dennler, G.; Scharber, M. C.; Brabec, C. J. Polymer-Fullerene Bulk-Heterojunction Solar Cells. *Adv. Mater.* **2009**, *21*, 1323−1338.
(104) Pandey, R.; Holmes, R. J. Graded Donor-Acceptor Heterojunctions for Efficient Organic Photovoltaic Cells. *Adv. Mater.* **2010**, *22*, 5301−5305.
(105) Wu, Y.; Yang, X.; Chen, W.; Yue, Y.; Cai, M.; Xie, F.; Bi, E.; Islam, A.; Han, L. Perovskite Solar Cells with 18.21% Efficiency And area over 1 Cm2 Fabricated by Heterojunction engineering. *Nat. Energy* **2016**, *1*, 16148.
(106) Marinova, N.; Valero, S.; Delgado, J. L. Organic and Perovskite Solar Cells: Working Principles, Materials and Interfaces. *J. Colloid Interface Sci.* **2017**, *488*, 373−389.
(107) Chen, P.; Wang, E.; Yin, X.; Xie, H.; Que, M.; Gao, B.; Que, W. Additive-Assisted One-Step Formed Perovskite/Hole Conducting Materials Graded Heterojunction for Efficient Perovskite Solar Cells. *J. Colloid Interface Sci.* **2018**, *532*, 182−189.

https://dx.doi.org/10.1021/acsami.9b18936
ACS Appl. Mater. Interfaces 2020, 12, 3736−3745